9

Research article

Gulnaz Rakhmanova and Ivan V. Iorsh*

Broadband enhancement of second-harmonic generation at the domain walls of magnetic topological insulators

https://doi.org/10.1515/nanoph-2020-0287 Received May 15, 2020; accepted September 9, 2020; published online September 25, 2020

Abstract: We show that the second-harmonic generation (SHG) is enhanced in the chiral one-dimensional electron currents in a broad frequency range. The origin of the enhancement is twofold: first, the linear dispersion of the quasiparticles and the associated plasmonic mode as well as the quasi-linear dispersion of plasmon-polariton result in the lift of the phase-matching condition. Moreover, the strong field localization leads to the further increase of the SHG in the structure. The results suggest that the chiral currents localized at the domain walls of magnetic topological insulators can be an efficient source of the second-harmonic signal in the terahertz frequency range.

Keywords: magnetic topological insulator; plasmon-polariton; second-harmonic generation.

1 Introduction

In recent years, the field of plasmonics has been enjoying the exploration of plasmonic excitations in novel topological materials [1–3]. The appeal of the topological materials for plasmonics is largely dictated by the fact that the topologically protected surface currents in these materials support plasmonic excitations inheriting the immunity to backscattering, resulting in the suppression of the net plasmonic loss rate, which is of paramount importance for enabling applications of plasmonics in various fields [4]. The field of topological plasmonics is now rapidly

evolving, and a plethora of novel low-loss plasmonic excitations have been predicted and observed in various topological insulators [5–9] and other topological materials, such as, e.g., Weyl semimetals [10–13].

One of the most promising applications of plasmonics is the enhancement of the nonlinear optical processes, specifically second-harmonic generation (SHG) and higher harmonic generation [14–17]. The amplification of the nonlinear signal is achieved owing to the plasmon-assisted field enhancement. One of the limiting factors for the harmonic generation efficiency is the ubiquitous ohmic losses. In this perspective, exploitation of topological plasmons with suppressed loss rates for the nonlinear frequency conversion could significantly enhance the conversion efficiencies.

Noteworthy, the topologically nontrivial photonic structures have been recently proposed for the enhancement of the higher harmonic generation (see the review by Smirnova et al. [18] and the references within). While in most of these studies the nonlinear current is produced by the conventional optically nonlinear media (such as lithium niobate or GaAs), the topologically nontrivial edge and surface states emerging in these structures facilitate the strong field enhancement, extended lifetime, and unidirectional mode propagation which cumulatively increase the conversion efficiency [19].

At the same time, it has been shown in a number of papers that the linear electronic dispersion arising in topologically protected surface states as well as in low-dimensional Dirac materials such as graphene may result in drastic enhancement of the nonlinear current [20–22].

Topological plasmon-polariton, composite quasiparticle, a superposition of the topologically protected surface or edge current and an electromagnetic field could thus provide a twofold source for the enhancement of the nonlinear signal since they emerge owing to the interaction of the electrons with linear dispersion, hence, with immunity to backscattering, and the subwavelengthly localized electromagnetic field.

In this letter, we exploit this simple idea by studying the SHG by the edge plasmon-polariton (EPP) localized at

Gulnaz Rakhmanova, ITMO University, Kronverkskiy Prospekt 49, Saint Petersburg 197101, Russia. https://orcid.org/0000-0001-8750-4065

^{*}Corresponding author: Ivan V. Iorsh, ITMO University, Kronverkskiy Prospekt 49, Saint Petersburg 197101, Russia,

E-mail: iorsh86@yandex.ru

the domain wall in the magnetic topological insulator (MTI).

The MTI can be realized, e.g., in the form of a ferromagnet thin film in close proximity to a surface of the 3D topological insulator or topological semimetal [23–25]. A perpendicular-to-plane magnetization component in the ferromagnet induces a finite effective mass of the otherwise massless surface electrons. This results in a bandgap in the spectrum of the surface states. A one-dimensional domain wall in the ferromagnet is, however, imaged in the Dirac electron system as a zero mass line that supports a helical electronic state. These quasi-one-dimensional edge states are characterized by the linear electron dispersion and are anomalous Hall counterparts of the quantum Hall edge states.

It has been recently demonstrated that the MTI can be realized in a single material without the need for the realization of the proximity effect, namely, in the study by Yin et al. [26], it has been shown that $TbMn_6Sn_6$ is characterized both by the topological surface states and finite magnetization, which results in the gap opening in the surface state spectrum. Notably, the width of the gap observed in this material (34 meV) is an order of magnitude larger than the gaps occurring owing to the proximity effects (1–2 meV).

In the study by Iorsh et al. [27], we have shown that these currents support a strongly localized low-loss helical plasmon-polaritons with almost linear dispersion. Here, we consider a SHG supported by this EPP mode, namely, we consider the situation shown schematically in Figure 1. A linear EPP is excited by a point-like scatterer (it may be a tip of the scattering near-field optical microscope [28–30]

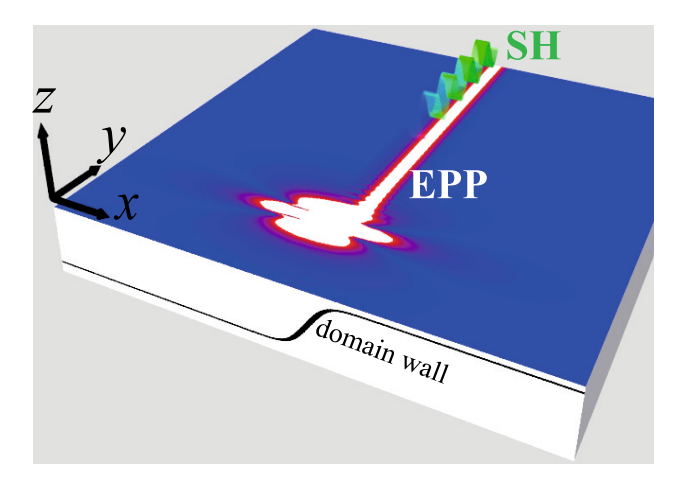


Figure 1: Scheme of the second-harmonic generation (SHG) by the chiral current in magnetic TI. A point dipole excited an edge plasmon-polariton (EPP) localized at the domain wall. Nonlinear conductivity results in the emergence of the SH signal, which is also localized at the domain wall. TI, topological insulator.

or a deeply subwavelength resonant nanoantenna [31]). We then calculate the nonlinear conductivity, nonlinear current and the intensity of the second-harmonic signal in this setup.

2 Results and discussion

A helical electronic state arising at the single domain wall in the MTI structure is described by the Hamiltonian:

$$\widehat{H} = v \left[\sigma \times \mathbf{p} \right]_z + \Delta \tanh \left(x/a_0 \right) \sigma_z, \tag{1}$$

where v is the Fermi velocity, Δ is the gap width proportional to the net magnetization, and a_0 is the width of the domain wall. The eigenenergies of the edge states are given simply by $E = \hbar v k_v$, and the eigenstates are given by

$$\Psi_{\nu}(x,y) = F_{\nu}(x) \frac{e^{iqy}}{\sqrt{2\pi}}, \quad F_{\nu}(x) = \frac{[a_0 B(1/2,\nu)]^{-\frac{1}{2}}}{\cosh^{\nu}(x/a_0)}, \quad (2)$$

where $v = a_0/l$, $l = \hbar v/\Delta$, and B is the Euler beta function. In the limit of the infinitely thin domain wall, $a_0 = 0$:

$$F(x) = F_0(x) = \frac{1}{\sqrt{l}} \exp\left[-\frac{|x|}{l}\right]. \tag{3}$$

In what follows, we assume that the Fermi energy lies in the center of the bulk gap and that the frequency of the electromagnetic field is smaller than the gap width $\hbar\omega<\Delta$. Within this approximation, we can neglect the excitation of the bulk states and assume that both linear and nonlinear currents are generated solely by the intraband transitions of the edge state. Both linear and nonlinear conductivities can be obtained within the unified formalism based on the density matrix approach, namely, the average current is given by

$$\langle \mathbf{J}(t) \rangle = \text{Tr}[\mathbf{J}\rho(t)] = \sum_{n} \frac{e^{-\beta E_{n}}}{Z} \langle n(t) | \hat{\mathbf{J}}(t) | n(t) \rangle,$$
 (4)

where **J** is the current operator, $\rho(t)$ is the density matrix operator, E_n and $|n(t)\rangle$ are the eigenvalues and eigenfunctions written in the interaction picture, respectively, and Z is the corresponding partition function. The time-dependent eigenstates in the interaction picture are simply $|n(t)\rangle = e^{-i\hbar \int_0^t dt' V(t')} |n\rangle$, where the interaction term is given by

$$V(t) = -ev[\sigma \times \mathbf{A}(t)], \tag{5}$$

where $\mathbf{A}(t)$ is the vector potential of the perturbing field. The current operator is found as $\mathbf{J} = \partial V/\partial \mathbf{A}(t)$. The linear conductivity of this system has been evaluated in the study by Iorsh et al. [27] and is written as:

$$\sigma_{yy}(\omega,q,x,x',z,z') = \frac{\alpha i}{2\pi} \frac{v^2 q}{\omega} \frac{F_{\nu}^2(x) F_{\nu}^2(x')}{(k_0 - \nu q/c)} \delta(z) \delta(z') \,, \eqno(6)$$

where α is the fine structure constant, $k_0 = \omega/c$, and F(x) is the function describing the transverse profile of the quasione-dimensional current. In the limit of the infinitely narrow domain F(x) is given by (3).

It can be seen that the linear dispersion has a resonance at the dispersion of the chiral plasmon $\omega = vq$. While these plasmons cannot be excited by a plane wave since their dispersion lies well below the light cone, they can be excited by a evanescent field of the point-like scatterers. The dressing of the chiral plasmon by the electromagnetic field leads to formation of plasmon-polariton defined by the equation [27]:

$$S(q,\omega) = 1 - \tilde{v}\tilde{q} - \alpha \tilde{v}^2 \tilde{q} \frac{(\tilde{q}^2 - 1)}{\Gamma^4(v)} \int_0^\infty dx \frac{|\Gamma(v(1 + ix/2))|^4}{\sqrt{q^2 l^2 + x^2 - k_0^2 l^2}} = 0,$$

which in the limit $a_0 = 0$ reduces to

$$S(q,\omega) = 1 - \tilde{v}\tilde{q} - \alpha \tilde{v}^2 \tilde{q} (\tilde{q}^2 - 1) \frac{(1 + \kappa^2) \tanh^{-1} \kappa - \kappa}{2\pi \kappa^3} = 0,$$
(8)

where $\tilde{v} = v/c$, $\tilde{q} = q/k_0$ and $\kappa^2 = 1 + (\hbar\omega/2\Delta)^2 \tilde{v}^2 (1 - \tilde{q}^2)$. The dispersion defined by Eq. (8) is shown in Figure 2(a).

We can see that the plasmon is weakly hybridized by the electromagnetic field and the dispersion of the plasmon-polariton is close to the one of plasmon. Moreover, we can see that for the reasonable values of v, the dispersion of EPP depends on ν only weakly. For the currently known experimental realizations of the MTI, the value of ν lies in the range $\nu \sim 10^{-2} - 10^{-1}$. We can see that at v = 0.1, the dispersion of EPP becomes indistinguishable from the one with v = 0. In what follows, we all assume v = 0 in the calculations. Finally, it can be seen that within the gap, the dispersion of the edge state is almost linear. Specifically, it becomes increasingly linear as ν approaches zero. Figure 2(b) shows the quantity describing the linearity of the dispersion $(q(2\omega) - 2q(\omega))/q(\omega)$. This quantity can be regarded as the dimensionless phase mismatch. It can be seen that as ν approaches zero, the phase mismatch is small across all of the gap regions. As shown in the study by Iorsh et al. [27], the structure excited by a point-like scatterer such as a tip of scattering SNOM would support a long-living quasione-dimensional plasmon-polariton with the dispersion defined by (8).

The nonlinear conductivity responsible for the SHG can be calculated straightforwardly from the expression

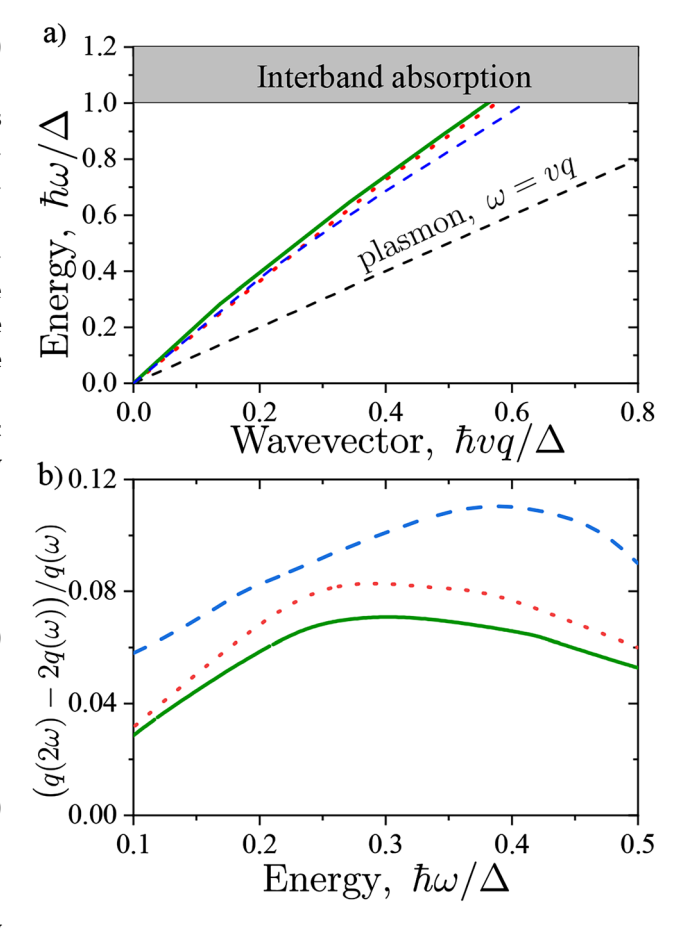


Figure 2: (a) Dispersion of the EPP for different values of v: v = 0.1(solid green), v = 0.5 (dotted red), and v = 1 (dashed blue). (b) The dimensionless parameter of the phase mismatch. The line legend is the same for figure (a). EPP, edge plasmon-polariton.

(4). The nonlocal nonlinear conductivity is found from the relation

$$J_{i}(x,2\omega,2q) = \iint dx_{1}dx_{2}\sigma_{ijk}^{SHG}(\omega,x,x_{1},x_{2},q)E_{\omega,j}(x_{1},q)E_{\omega,k}(x_{2},q)$$
(9)

The details of the calculation can be found in Appendix A, and the expression for σ_{nl} is given by:

$$\sigma_{yyy}^{SHG} = \frac{c}{e} \tilde{q} \frac{\alpha^2 \tilde{v}^3}{2\pi} \frac{k_0^{-3} F^2(x) F^2(x_1) F^2(x_2)}{(1 - \tilde{v}\tilde{q})^2} \,. \tag{10}$$

We see that according to the symmetry restrictions, since our system possesses the center of symmetry, the second-harmonic current should be proportional to the wavevector of light in the direction of propagation [32], $J(2\omega) \sim E^2 \tilde{q}$.

In calculation of the linear and nonlinear conductivity, we have neglected the processes of photoionization, i.e., the direct transitions between the edge states and the bulk states in the conduction and valence bands. This approximation is valid when (for the case of the Fermi energy in the center of the gap) $2\omega < \Delta$. Moreover, unlike the case of the spin Hall effect edge currents, there is only one edge state per edge; thus, direct optical transitions between two edge states with opposite helicities do not occur. In order to avoid the thermal excitation of the bulk states, we also consider the limit $T \ll \Delta$. The only source of the spreading of the electron wavepacket is thus the momentum relaxation of the chiral electrons in the channel due to impurity scattering, which is weak in the quantum Hall edge currents.

We now consider the situation similar to one considered in the study by Iorsh et al. [27]: a helical EPP is excited by a point-like scatterer and propagates along the domain wall. At the sufficient distance from the scatterer, the profile electric field is dominantly defined by the field of the EPP. Its y component, the only one responsible for the nonlinear current generation, reads for the plane z = 0:

$$E_{\nu}^{\text{EPP}}(x,y) = E_0 \mathcal{E}(\omega, q_{EP}, x) e^{iq_{EP}y}, \qquad (11)$$

where E_0 is the amplitude defined by the coupling efficiency of the point-scatterer field to the EPP mode, $q_{EP}(\omega)$ is the wave vector of the EPP, defined by Eq. (8), and dimensionless functions \mathcal{E} define the profile of the field:

$$\mathcal{E}(\omega, q, x) = \int dx' G(x - x', \omega, q) F^{2}(x'), \qquad (12)$$

where the Green's function *G* is given by

$$G_{yy}(x-x',\omega,q) \sim K_0 \left(\sqrt{q^2 - k_0^2} |x-x'| \right),$$
 (13)

where K₀ is the Macdonald function.

According to Eq. (9), the nonlinear current can be written as

$$J_{y}(x,2\omega,y) = \frac{c}{e}\tilde{q}_{EP}\frac{\alpha^{2}\tilde{v}^{3}}{2\pi} \frac{F^{2}(x)E_{0}^{2}\Lambda^{2}(\omega,q_{EP})}{k_{0}^{3}(1-\tilde{v}\tilde{q}_{EP})^{2}} e^{2iq_{EP}y}, \quad (14)$$

where $\Lambda(\omega, q) = \int dx F^2(x) \mathcal{E}(\omega, q, x)$. The bare field at second harmonic can then be written as

$$E_{\text{bare}}(2\omega, x, y) = E_{2\omega} \mathcal{E}(2\omega, 2q_{FP}, x). \tag{15}$$

However, the electric field at the second harmonic also gets renormalized owing to the hybridization with the linear EPPs at the second harmonic. Collecting all the terms together, we get the expression for the electric field at the second harmonic:

$$E_{y}(x,2\omega,y)e^{-2iq_{EP}y} = R(\omega)\frac{\alpha\tilde{v}}{ek_{0}^{2}}E_{0}^{2}\mathcal{E}(2\omega,q_{EP},x), \qquad (16)$$

where

$$R(\omega) = \left[1 + \frac{\alpha \tilde{\mathbf{v}} \Lambda(2\omega, 2q_{EP})}{S(2q_{EP}, 2\omega)}\right] \frac{2\tilde{q}_{EP} \alpha \tilde{\mathbf{v}}^2 \Lambda^2(\omega, q_{EP})}{(1 - \tilde{\mathbf{v}}\tilde{q}_{EP})^2}, \quad (17)$$

where S is defined by Eq. (8).

The profiles of the E_y field component in the xz plane for frequencies $\hbar\omega/\Delta=1/3$ and $\hbar\omega/\Delta=2/3$ are shown in Figure 3(a and b), respectively. It can be seen that the field is distorted in the x direction owing to the finite localization length l of the topological current and that the field at second harmonic is more localized.

Different terms entering Eq. (17) are plotted in Figure 3(c), namely, the term S in the denominator can be regarded as the phase-matching factor. Naturally, owing to the almost linear dispersion of the EPP, S is quite small, and the resonant contribution to the SHG signal is significant. The terms Λ correspond to the field enhancement due to the subwavelength field localization in the EPP mode. The function Λ has a logarithmic divergence in the limit of low frequencies. This however can be regularized either by introducing small but finite skin depth of the edge current in the z direction or introducing a low frequency cutoff which is done further in the manuscript. The value of $R(\omega)$, which cumulatively includes contributions from Λ and 1/S, is of the order of 10^{-3} in the broad frequency range.

Omitting the spatial profiles, the ratio of the field amplitudes at the second and fundamental harmonic can be presented as

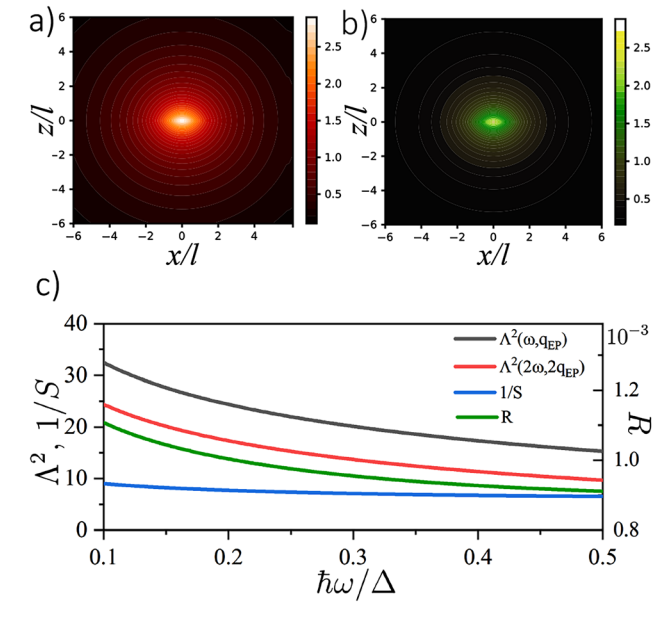


Figure 3: Profiles of the E_y component of the EPP field at $\hbar\omega/\Delta=1/3$ (a) and $\hbar\omega/\Delta=2/3$ (b). (c) Spectrum of different contributions to the SHG enhancement factor R. EPP, edge plasmon-polariton; SHG, second-harmonic generation.

$$E_{\rm SHG}/E_0 = R(\omega) \left[\frac{eE_0 v/\omega}{\hbar \omega} \right].$$
 (18)

We can see that the efficiency of the SHG is proportional to the ratio of the maximum kinetic energy gain by electron per the EM field period and the photon energy. First, let us recall that in the conventional conducting systems in the limit of low frequencies, the mean momentum is proportional to the relaxation time τ rather than to the field period. The relaxation time τ is defined by the impurityassisted backscattering and by the thermal fluctuationassisted ionization of the edge state electrons to the bulk conduction band. The latter processes are suppressed by a factor $\exp[-\Delta/(k_BT)]$, which can be vanishingly small for low temperatures. The former process is suppressed in the anomalous Hall regime since there is no backpropagating state. This is in stark contrast to the case of spin Hall regime, where there are two counter-propagating edge states with opposite spins, and thus any magnetized impurity or even electron-electron interactions can result in effective momenutm relaxation. We thus argue that for the case of anomalous Hall plasmon-polaritons, the upper limit for the nonlinear response is defined not by the internal losses, but rather by the finite size of the domain wall. Specifically, it is evident that when the kinetic energy gain per EM cycle exceeds Δ , the electrons reach the bulk conduction band and that our approximations cannot be applied. It means that the upper limit for the numerator of the bracketed expression in Eq. (18) is Δ . At the same time, we have considered the infinitely long domain wall. This approximation holds when the longitudinal extent of the domain wall L is much larger than the effective wavelength of the plasmon-polariton, which can be approximated by $\lambda_{EP} \sim 2\pi v/\omega$. With this, we can estimate the upper limit for the quantity in brackets:

$$Q(\omega) = \left[\frac{eE_0 \nu/\omega}{\hbar \omega} \right] < \frac{\Delta L}{2\pi \hbar \nu} = \frac{L}{2\pi l}.$$
 (19)

For the domain wall length of 10 µm, the dimensionless quantity can be as large as 20. For the adequate electric field amplitudes, a more accurate approximation may be made, namely, the characteristic timescale is defined not by momentum relaxation τ but rather by the time $\tau_0 = L/\nu$ taken by the electron to travel along the whole domain wall. In this case, we can write

$$Q(\omega) < \frac{eE_0L}{\Delta} \frac{L}{2\pi l} = \frac{eE_0L^2}{2\pi\hbar\nu}.$$
 (20)

Let us consider the specific case of $\hbar\omega = 0.5 \,\mathrm{meV}$, $\Delta = 1.5 \,\mathrm{meV}$, and v = c/600. In this case, $l = \approx 160 \,\mathrm{nm}$. We also assume $L=10~\mu m$. In this case, $\tau_0 \approx 20~ps$ and $T = 2\pi/\omega \approx 10 \text{ ps} \approx \tau_0$. In this case, for a moderate field amplitude of 1V/cm $Q(\omega) \approx 6.5$. Multiplying it by the respective value of R, we can estimate the effective nonlinear susceptibility as 7×10^{-3} cmV⁻¹, which is five orders of magnitude larger than in the bulk GaAs, 1.7 \times 10⁻⁸ [cm/V] [33], four orders of magnitude larger than in the GaAs quantum well, $\sim 10^{-7}$ [cm/V] [33], and three orders of magnitude larger than in graphene, $\sim 10^{-6} [\text{cm/V}] [21]$. It is also considerably stronger than the nonlinear response of noncentrosymmetric topological insulators [34, 35], 10⁻⁶ [cm/V]. These structures are however two dimensional in contrast to our one-dimensional structure, and thus, the coupling efficiency of the far-field radiation should be accounted for. The efficiency of coupling of the field of fundamental harmonic to the EPP mode is of the order of 10⁻². The coupling efficiency can be improved by using not a point source, but a diffraction grating with a period much less than the wavelength and with the reciprocal grating vector is equal to the EPP wavelength. There are now many other routes of efficient coupling of the bulk field to the deeply subwavelength plasmonic terahertz modes [36]. This suggests that the chiral currents may be regarded as an extremely efficient source of SHG in the terahertz range.

We stress that the aforementioned response is broadband and does not require any additional photonic resonant structure, while it is evident that the latter would further increase the SHG signal. In the estimation of the effective nonlinear response, we did not account for the efficiency of coupling of the fundamental harmonic signal to the EPP mode, which is usually weak owing to the strong localization of the EPP. It is also noteworthy that the broadband response is achieved owing to the almost linear dispersion of EPPs in the structure providing the lift of the strict phase-matching conditions.

To conclude, we have considered the SHG in the chiral current localized at the domain wall of the MTI. Assisted by the excitation of the edge plasmon-polariton both at fundamental harmonic and second-harmonic frequency, the SHG process can be several orders more efficient than in graphene, in two-dimensional and bulk GaAs φτ. The effect is broadband due to the linear dispersion of both the current and plasmon-polariton mode, and owing to the absence of the backscattering in the chiral current, its magnitude is virtually limited only by the domain wall length. Thus, we anticipate that the nanostructures comprising domain walls in the MTI can become a building block for the efficient sources of SHG in the terahertz range.

Acknowledgments: We acknowledge the support from the Russian Science Foundation, under Project 20-12-00224, and RFBR, project number 20-32-70185.

Author contribution: All the authors have accepted responsibility for the entire content of this submitted manuscript and approved submission.

Research funding: The reported study was funded by Russian Science Foundation (Project No. 20-12-00224) and RFBR (project number 20-32-70185).

Conflict of interest statement: The authors declare no conflicts of interest.

Appendix A Derivation of the expression for the nonlinear conductivity

The average current is given by (4), where the time evolution operator:

$$\widehat{U}(t,t_{0}) = e^{-i/\hbar \int_{t_{0}}^{t} dt' V(t')} = 1 + \frac{1}{i} \int_{t_{0}}^{t} dt_{1} \widehat{V}(t_{1})$$

$$+ \frac{1}{i^{2}} \int_{t_{0}}^{t} dt_{1} \widehat{V}(t_{1}) \int_{t_{0}}^{t_{1}} dt_{2} \widehat{V}(t_{2})$$
(A.1)

The interaction term is represented in a form $\widehat{V}(t,r) = \widehat{V}_0(t,r) + \widehat{V}_0^{\dagger}(t,r)$. Specifically,

$$V(t,r) = -ev[\sigma \times \mathbf{A}(t,r)], \tag{A.2}$$

where $\mathbf{A}(t)$ is the vector potential of the perturbing field and equal to:

$$\mathbf{A}(t,r) = \mathbf{A}e^{-i\omega t + iqr} + \mathbf{A}^* e^{i\omega t - iqr}$$
 (A.3)

In the second order, there are two contributions to the nonlinear current:

$$\langle J_2 \rangle \approx \langle n|J_2(t)|n\rangle + \langle n_1(t)|J(t)|n_1(t)\rangle,$$
 (A.4)

Here, the first one comes from the averaging of the secondorder perturbation of the current operator over the equilibrium distribution. From the Baker-Campbell-Hausdorff formula, $J_2 \sim [J, V(t_1), V(t_2)]_+$. The second one comes from the averaging over the equilibrium current operator over the first-order correction to the eigenstates.

Besides, the SHG, the second-order response allows for the generation of the dc current. These terms would be proportional to AA*, A*A.

The first term in Eq. (A.4) results in the zero dc current (for the case of linear dispersion of the electron eigenstates), and the contribution to the second harmonic is given by

$$\langle \mathbf{J} \rangle_{2\omega,2q}^{(1)}(x,x') = \sum_{n} [f_n + f_{n+2q}]$$

$$\times \frac{-e^3 v_F^3 F^2(x) F^2(x_1) F^2(x_2) \mathbf{A}^2}{(E(k_n+q) - E(k_n) - \omega) (E(k_n+2q) - E(k_n) - 2\omega)}$$
(A.5)

The analogous term comes for $J_{-2\omega,-2a}$.

The contribution from the second term in Eq. (A.4) is given by

$$\langle \mathbf{J} \rangle_{2\omega,2q}^{(2)}(x,x') = e^{3} v_{F}^{3} \sum_{n} f_{n}$$

$$\times \frac{F^{2}(x_{1})F^{2}(x)F^{2}(x'_{1})\mathbf{A}^{2}}{(E(k_{n}) - E(k_{n} - q) - \omega)(E(k_{n} + q) - E(k_{n}) - \omega)}$$
(A.6)

We then sum the contributions in Eqs. (A.5) and (A.6) and assume the low temperature limit, when $f_n = \Theta(-k_n)$, the Heaviside function. In this limit, the summation over n is readily vielding the final answer presented in the main manuscript

$$\begin{split} \sigma_{yyy}^{SHG}\left(\omega_{0},q\right) &= \frac{1}{\omega_{0}^{2}} \frac{e^{3}v_{F}^{3}}{c^{2}\hbar^{2}} \frac{F^{2}(x)F^{2}(x_{1})F^{2}(x_{2})}{\left(-v_{F}q/c+k_{0}\right)^{2}} \frac{q}{2\pi} \\ &= \frac{c}{e} \tilde{q} \frac{\alpha^{2}\tilde{v}_{F}^{3}}{2\pi} \frac{k_{0}^{-3}F^{2}(x)F^{2}(x_{1})F^{2}(x_{2})}{\left(1-\tilde{v}\tilde{q}\right)^{2}} \,, \end{split} \tag{A.7}$$

 $k_0 = \omega_0/c$ $\tilde{q} = q/k_0$ v&doublehyphen; 3pt&doublehyphen; 5.5pt~ $_{E} = v_{E}/c$, $\alpha = e^2/c\hbar$.

The contribution to the dc current from the second term in Eq. (A.4) is given by

$$\sigma_{2,dc}(\omega,q) = -\sum_{m} [f(k_m + q) + f(k_m - q)] \times \frac{e^3 v_F^3 F^2(x_1) F^2(x) F^2(x_1')}{\hbar^2 (v_E q - \omega)^2}$$
(A.8)

References

- [1] Y.-P. Lai, I.-T. Lin, K.-H. Wu, and J.-M. Liu, "Plasmonics in topological insulators," Nanomater. Nanotechnol., vol. 4, p. 13, 2014.
- [2] T. Stauber, "Plasmonics in dirac systems: from graphene to topological insulators," J. Phys. Condens. Matter, vol. 26, p. 123201, 2014.
- T. Stauber, G. Gómez-Santos, and L. Brey, "Plasmonics in topological insulators: spin-charge separation, the influence of the inversion layer, and phonon-plasmon coupling," ACS Photonics, vol. 4, p. 2978, 2017.
- [4] A. Boltasseva and H. Atwater, "Low loss plasmonic metamaterials," Science, vol. 331, p. 290, 2011.
- J. C. W. Song and M. S. Rudner, "Chiral plasmons without magnetic field," Proc. Natl. Acad. Sci. U. S. A., vol. 113, p. 4658, 2016.

- [6] A. Kumar, A. Nemilentsau, K. H. Fung, G. Hanson, N. X. Fang, and T. Low, "Chiral plasmon in gapped dirac systems," Phys. Rev. B, vol. 93, p. 041413, 2016.
- [7] P. Di Pietro, M. Ortolani, O. Limaj, et al., "Observation of dirac plasmons in a topological insulator," Nat. Nanotechnol., vol. 8, p. 556, 2013.
- [8] M. Autore, F. D'Apuzzo, A. Di Gaspare, et al., "Plasmon-phonon interactions in topological insulator microrings," Adv. Opt. Mater., vol. 3, p. 1257, 2015.
- [9] D. Jin, L. Lu, Z. Wang, et al., "Topological magnetoplasmon," Nat. Commun., vol. 7, p. 13486, 2016.
- [10] F. M. D. Pellegrino, M. I. Katsnelson, and M. Polini, "Helicons in weyl semimetals," Phys. Rev. B, vol. 92, p. 201407, 2015.
- [11] J. Hofmann and S. Das Sarma, "Surface plasmon polaritons in topological weyl semimetals," Phys. Rev. B, vol. 93, p. 241402, 2016.
- [12] J. C. Song and M. S. Rudner, "Fermi arc plasmons in weyl semimetals," Phys. Rev. B, vol. 96, p. 205443, 2017.
- [13] G. M. Andolina, F. M. D. Pellegrino, F. H. L. Koppens, and M. Polini, "Quantum nonlocal theory of topological fermi arc plasmons in weyl semimetals," Phys. Rev. B, vol. 97, p. 125431, 2018.
- [14] S. Kim, J. Jin, Y.-J. Kim, I.-Y. Park, Y. Kim, and S.-W. Kim, "Highharmonic generation by resonant plasmon field enhancement," Nature, vol. 453, p. 757, 2008.
- [15] I.-Y. Park, S. Kim, J. Choi, et al., "Plasmonic generation of ultrashort extreme-ultraviolet light pulses," Nat. Photonics, vol. 5, p. 677, 2011.
- [16] N. Pfullmann, C. Waltermann, M. Kovačev, et al., "Nanoantenna-assisted harmonic generation," Appl. Phys. B, vol. 113, p. 75, 2013.
- [17] A. de Hoogh, A. Opheij, M. Wulf, N. Rotenberg, and L. Kuipers, "Harmonics generation by surface plasmon polaritons on single nanowires," ACS Photonics, vol. 3, p. 1446, 2016.
- [18] D. Smirnova, D. Levkam, Y. Chong, and Y. Kivshar, "Nonlinear topological photonics," 2019, arXiv:1912.01784 [physics.optics].
- [19] D. Smirnova, S. Kruk, D. Leykam, E. Melik-Gaykazyan, D.-Y. Choi, and Y. Kivshar, "Third-harmonic generation in photonic topological metasurfaces," Phys. Rev. Lett., vol. 123, p. 103901, 2019.
- [20] S. A. Mikhailov, "Theory of the giant plasmon-enhanced secondharmonic generation in graphene and semiconductor twodimensional electron systems," Phys. Rev. B, vol. 84, p. 045432, 2011.
- [21] M. M. Glazov, "Second harmonic generation in graphene," JETP Lett. (Engl. Transl.), vol. 93, p. 366, 2011.

- [22] J. W. McIver, D. Hsieh, S. G. Drapcho, et al., "Theoretical and experimental study of second harmonic generation from the surface of the topological insulator bi2se3," Phys. Rev. B, vol. 86, p. 035327, 2012.
- [23] A. T. Lee, M. J. Han, and K. Park, "Magnetic proximity effect and spin-orbital texture at the bi2se3/EuS interface," Phys. Rev. B, vol. 90, p. 155103, 2014.
- [24] C. Lee, F. Katmis, P. Jarillo-Herrero, J. S. Moodera, and N. Gedik, "Direct measurement of proximity-induced magnetism at the interface between a topological insulator and a ferromagnet," Nat. Commun., vol. 7, p. 12014, 2016.
- [25] J. Hu, Z. Tang, J. Liu, Y. Zhu, J. Wei, and Z. Mao, "Nearly massless dirac fermions and strong zeeman splitting in the nodal-line semimetal zrsis probed by de haas-van alphen quantum oscillations," Phys. Rev. B, vol. 96, p. 045127, 2017.
- [26] J.-X. Yin, W. Ma, T. A. Cochran, et al., "Quantum-limit chern topological magnetism in tbmn 6 sn 6," Nature, vol. 583, p. 533, 2020.
- [27] I. Iorsh, G. Rahmanova, and M. Titov, "Plasmon-polariton from a helical state in a dirac magnet," ACS Photonics, vol. 6, p. 2450,
- [28] J. Chen, M. Badioli, P. Alonso-González, et al., "Optical nanoimaging of gate-tunable graphene plasmons," Nature, vol. 487, p. 77, 2012.
- [29] Z. Fei, A. Rodin, G. Andreev, et al., "Gate-tuning of graphene plasmons revealed by infrared nano-imaging," Nature, vol. 487, p. 82, 2012.
- [30] D. Basov, M. Fogler, and F. G. de Abajo, "Polaritons in van der waals materials," Science, vol. 354, p. 6309, 2016.
- [31] Y. Li, M. Kang, J. Shi, K. Wu, S. Zhang, and H. Xu, "Transversely divergent second harmonic generation by surface plasmon polaritons on single metallic nanowires," Nano Lett., vol. 17, p. 7803, 2017.
- [32] M. V. Durnev and S. A. Tarasenko, "High-frequency nonlinear transport and photogalvanic effects in 2d topological insulators," Ann. Phys., vol. 531, p. 1800418, 2019.
- [33] D. Nelson and M. Delfino, Nonlinear Dielectric Susceptibilities, Springer-Verlag Berlin Heidelberg; 2000.
- [34] P. E. Ashby and J. P. Carbotte, "Tracking quasiparticle energies in graphene with near-field optics," Phys. Rev. B Condens. Matter, vol. 86, p. 1, 2012.
- [35] Z. Li and F. Nori, "Nonlinear response in a noncentrosymmetric topological insulator," Phys. Rev. B, vol. 99, p. 1, 2019.
- [36] Y.-M. Bahk, D. J. Park, and D.-S. Kim, "Terahertz field confinement and enhancement in various sub-wavelength structures," J. Appl. Phys., vol. 126, p. 120901, 2019.